# Probing active-sterile neutrino transition magnetic moments at LEP and CEPC

Yu Zhang[1] and Wei Liu[2,*]

[1]School of Physics, Hefei University of Technology, Hefei 230601, People's Republic of China
[2]Department of Applied Physics and MIIT Key Laboratory of Semiconductor Microstructure and Quantum Sensing, Nanjing University of Science and Technology, Nanjing 210094, People's Republic of China

(Received 29 January 2023; accepted 8 May 2023; published 22 May 2023)

We consider the sterile neutrino, which is also known as heavy neutral lepton, interacting with the Standard Model (SM) active neutrino and photon via a transition magnetic moment, the so-called dipole portal, which can be induced from the more general dipole couplings which respect the full gauge symmetries of the SM. Depending on the interactions with $\mathrm{SU}(2)_L$ and $\mathrm{U}(1)_Y$ field strength tensors $\mathcal{W}^a_{\mu\nu}$ and $B^{\mu\nu}$, we consider four typical scenarios and probe the constraints on the couplings with photon $d_\gamma$ at LEP using the analyses to search monophoton signature and the measurement of $Z$ decay. We find that in the considered scenarios assuming the coupling with $Z$ boson $d_Z \neq 0$, the measurement of $Z$ decaying into photon plus invisible particles can provide stricter constraints than the monophoton searches at the LEP1. The complementary constraints to existing experiments can be provided by the LEP. We also investigate the sensitivity on the dipole portal coupling $d_\gamma$ from the monophoton searches at future electron colliders, such as CEPC, and find that CEPC can explore the previously unconstrained parameter space by current experiments.

DOI: 10.1103/PhysRevD.107.095031

## I. INTRODUCTION

The discovery that neutrinos oscillate, and therefore have distinct mass and flavor eigenstates, has proven to be one of the most definitive pieces of evidence for physics beyond the Standard Model (BSM) in the past two decades [1,2]. Given that the Standard Model (SM) does not predict the observed small and nonzero neutrino masses, it is reasonable to introduce new physics which is typically organized in terms of the new particles and/or interactions. One feature present in many theories explaining neutrino masses is the addition of one or more heavy neutral leptons (HNLs) $N$, which can connect with neutrino masses via a Yukawa interaction, $\mathcal{L} \supset NHL$, and have attracted significant attentions in the past few years [3–13]. These neutral fermionic states $N$ are singlet under the SM gauge groups, and often referred to as the so-called sterile neutrinos or right-handed neutrinos.

One of the consequences of extending the SM with additional sterile neutrinos is that the neutrino magnetic moment is generated with a tiny value proportional to the neutrino mass [14–17]. Recently, such scenarios predicting HNLs with the dipole coupling to SM active neutrinos, which are allowed to offer novel signatures and features in the production and decay of $N$ if the traditional neutrino portal coupling $NHL$ is assumed to be absent or subdominant, have received renewed attention and have been studied in the context of colliders, beam-dump and neutrino experiments, astrophysics, cosmology, and direct searches at dark matter experiments [18–45]. At the effective low-energy level, the neutrino dipole portal to HNLs is described by the Lagrangian

$$\mathcal{L} \supset d_k \bar{\nu}^k_L \sigma_{\mu\nu} F^{\mu\nu} N + \mathrm{H.c.}, \tag{1}$$

where $k = e, \mu, \tau$ denotes the flavor index of the lepton, $\nu_L$ is a SM left-handed (active) neutrino field, $\sigma_{\mu\nu} = \frac{i}{2}[\gamma_\mu, \gamma_\nu]$, $F^{\mu\nu}$ is the electromagnetic field strength tensor, and $d$ is the active-sterile neutrino transition magnetic moment that controls the strength of the interaction with the units of $(\mathrm{mass})^{-1}$.

If the typical momentum exchange is much smaller than the electroweak scale, only considering the dipole portal coupling to sterile-active neutrinos and electromagnetic field strength tensor in the simplified model in Eq. (1) at the effective low-energy level is suitable. While scattering energy can be comparable with or above the electroweak

*wei.liu@njust.edu.cn
wei.liu.16@ucl.ac.uk

TABLE I. Four typical scenarios considered in this work.

| Scenario | Assumptions | Relations |
|---|---|---|
| I | $d_{\mathcal{W}} = 0$ | $d_Z = -d_\gamma \tan\theta_w$; $d_W = 0$ |
| II | $d_B = 0$ | $d_Z = d_\gamma \cot\theta_w$; $d_W = \sqrt{2} d_\gamma / \sin\theta_w$ |
| III | $d_{\mathcal{W}} = 2\tan\theta_w \times d_B$ | $d_Z = 0$; $d_W = \sqrt{2} d_\gamma \sin\theta_w$ |
| IV | $d_{\mathcal{W}} = -2\tan\theta_w \times d_B$ | $d_Z = -d_\gamma \tan(2\theta_w)$; $d_W = -\sqrt{2} d_\gamma \sin\theta_w / \cos(2\theta_w)$ |

scale, the SM gauge invariant dipole couplings should be taken into account [24,46]. The main aim of this study is to investigate the active-sterile neutrino transition magnetic moments which respect to the full gauge symmetries of the SM, and to probe the corresponding sensitivity at the electron colliders with the center-of-mass (c.m.) energy $\sqrt{s} \gtrsim M_Z$, such as LEP and future Circular Electron Positron Collider (CEPC) [47,48].

The paper is organized as follows. In Sec. II, we describe the model including the effective Lagrangian for the dipole portal coupling to HNLs. The production of sterile neutrino $N$ at electron colliders is investigated in Sec. III. We then discuss the constraints from LEP in Sec. IV, and from future CEPC in Sec. V. Section VI contains our discussion and conclusion.

## II. THE MODEL

It is worth noting that the effective Lagrangian in Eq. (1), describing the active-sterile neutrino transition magnetic moments, is not gauge invariant under the $\mathrm{SU}(2)_L \times \mathrm{U}(1)_Y$ gauge group. In order to describe the new physics above the electroweak scale, neutrino dipole couplings which respect the full gauge symmetries of the standard model need to be considered and can be written as [24]

$$\mathcal{L} \supset \bar{L}^k (d^k_{\mathcal{W}} \mathcal{W}^a_{\mu\nu} \tau^a + d^k_B B^{\mu\nu}) \tilde{H} \sigma_{\mu\nu} N + \mathrm{H.c.}, \tag{2}$$

where $\tilde{H} = i\sigma_2 H^*$, $\tau^a = \sigma^a/2$ with $\sigma^a$ being Pauli matrices, $\mathcal{W}^a_{\mu\nu}$ and $B^{\mu\nu}$ denote the $\mathrm{SU}(2)_L$ and $\mathrm{U}(1)_Y$ field strength tensors with $\mathcal{W}^a_{\mu\nu} \equiv \partial_\mu \mathcal{W}^a_\nu - \partial_\nu \mathcal{W}^a_\mu + g\epsilon^{abc} W^b_\mu W^c_\nu$ and $B_{\mu\nu} \equiv \partial_\mu B_\nu - \partial_\nu B_\mu$. It can be seen that, because of a Higgs insertion, the dipole interaction in Eq. (2) is really a dimension-6 operator. The Lagrangian in Eq. (2) can also be described with the Wilson coefficients $C_B$ and $C_{\mathcal{W}}$ by the replacement of $d_B \sim \frac{C_B}{\Lambda^2}$ and $d_{\mathcal{W}} \sim \frac{C_{\mathcal{W}}}{\Lambda^2}$, where $\Lambda$ is the cutoff energy scale.

After electroweak symmetry breaking (EWSB) with the Higgs vacuum expectation value $v$, one obtains

$$\mathcal{L} \supset d^k_W (\bar{\ell}^k W^-_{\mu\nu} \sigma_{\mu\nu} N) + \bar{\nu}^k_L (d^k_\gamma F_{\mu\nu} - d^k_Z Z_{\mu\nu}) \sigma_{\mu\nu} N + \mathrm{H.c.}, \tag{3}$$

which can induce dipole operators to the SM photon, the weak boson $Z$ and $W$, with the coupling $d^k_\gamma$, $d^k_Z$, and $d^k_W$. One sees that the normalization of the photon field strength term in Eq. (3) can induce that of Eq. (1). The active to sterile transition magnetic moment $d^k_\gamma$ is anticipated to be of order $\sim \frac{ev}{\Lambda^2}$, where $v$ is the Higgs field vacuum expectation value. For a given lepton flavor, the dipole couplings $d_\gamma$, $d_Z$, and $d_W$ in the broken phase are linearly dependent, and determined by only two parameters, $d_{\mathcal{W}}$ and $d_B$, in the unbroken phase via[1]

$$\begin{aligned} d_\gamma &= \frac{v}{\sqrt{2}} \left( d_B \cos\theta_w + \frac{d_{\mathcal{W}}}{2} \sin\theta_w \right), \\ d_Z &= \frac{v}{\sqrt{2}} \left( \frac{d_{\mathcal{W}}}{2} \cos\theta_w - d_B \sin\theta_w \right), \\ d_W &= \frac{v}{\sqrt{2}} \frac{d_{\mathcal{W}}}{2} \sqrt{2}. \end{aligned} \tag{4}$$

One finds that we have three free parameters in this model,

$$\{m_N, d_{\mathcal{W}}, d_B\}, \tag{5}$$

where $m_N$ is the mass of HNL. Assuming $d_{\mathcal{W}} = a \times d_B$, we have

$$\begin{aligned} d_Z &= \frac{d_\gamma (a\cos\theta_w - 2\sin\theta_w)}{2\cos\theta_w + a\sin\theta_w}, \\ d_W &= \frac{\sqrt{2} a d_\gamma}{2\cos\theta_w + a\sin\theta_w}. \end{aligned} \tag{6}$$

Then the independent parameters of (5) can be replaced by the parameters

$$\{m_N, d_\gamma, a\}. \tag{7}$$

In this work, we will focus on four typical scenarios, which are listed in Table I. In order to investigate the operators with $B_\mu$ and $\mathcal{W}_\mu$ individually, we consider $d_B = 0$ ($C_B = 0$) or $d_{\mathcal{W}} = 0$ ($C_{\mathcal{W}} = 0$) in scenarios I and II, respectively. One sees that scenario I with $a = 0$ leads to the coupling with the $W$ boson $d_W = 0$ after EWSB. With $d_B = 0$,

[1]As we will mostly assume that only one of the active neutrino flavors participates in the magnetic moment interactions, the superscript $k$ of the lepton flavor will be omitted in the following to simplify our notation, unless otherwise stated.

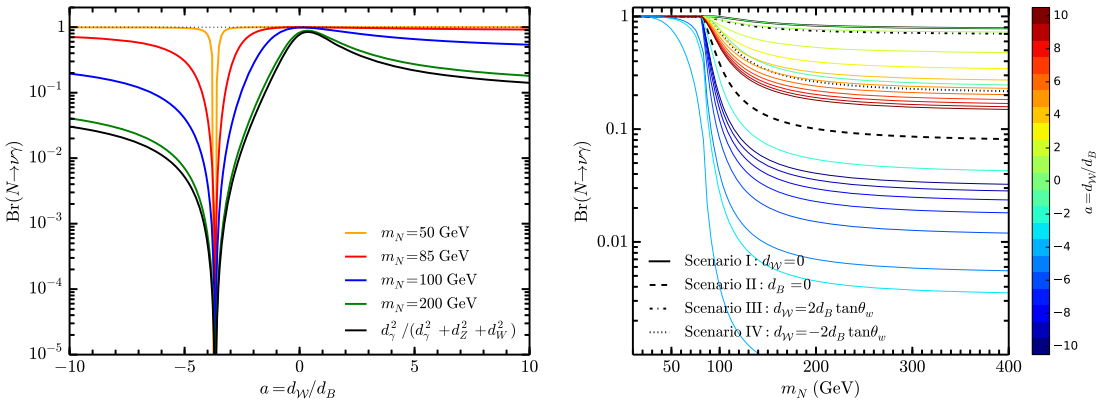


FIG. 1. Branching ratio of the radiative HNL decay process $N \to \nu\gamma$ as the ratio $a = d_W/d_B$ (left) and the function of the HNL mass $m_N$ (right).

scenario II corresponds to $a = d_W/d_B \to \infty$. We also consider scenario III in which $a = 2\tan\theta_w$ results in that the coupling with $Z$ boson $d_Z$ vanishing. For comparison, in scenario IV we set $a = -2\tan\theta_w$, which is the negative value in scenario III.

In general, the gauge invariant operators can generate neutrino masses at the dim-6 level with a Majorana mass term $\mathfrak{m}_N$ via loop diagrams. In this work, we consider the sterile neutrino $N$ as a Dirac fermion, then the sterile neutrino is decoupled from the mechanism that generates active neutrino masses. Large dipole couplings can be made compatible with small neutrino masses if the $N$ is Dirac, or quasi-Dirac with a small Majorana-type mass splitting satisfying $\mathfrak{m}_N \ll m_N$ [24].

The sterile neutrino $N$ as a Dirac fermion can decay into an on-shell vector boson and a SM lepton through the dipole operators in Eq. (3), with the decay rates given by

$$\begin{aligned}
\Gamma_{N\to\nu\gamma} &= \frac{d_\gamma^2 m_N^3}{4\pi},\\
\Gamma_{N\to\nu Z} &= \frac{d_Z^2(m_N^2 - M_Z^2)^2(2m_N^2 + M_Z^2)}{8\pi m_N^3}\Theta(m_N > M_Z),\\
\Gamma_{N\to W\ell} &= \frac{d_W^2}{8\pi m_N^3}\sqrt{(m_N^2 - (M_W - m_\ell)^2)(m_N^2 + (M_W - m_\ell)^2)}\\
&\quad\times(2m_\ell^2(2m_\ell^2 - 4m_N^2 - M_W^2) + (m_N^2 - M_W^2)\\
&\quad\times(2m_N^2 + M_W^2))\Theta(m_N > M_W + m_\ell). \qquad (8)
\end{aligned}$$

Besides, there will be three-body decay channels of HNL via off-shell $W$ and $Z$ bosons, such as $N \to W^*\ell \to \ell + ff'$ and $N \to \nu Z^* \to \nu f\bar{f}$, which are suppressed by a factor of fine structure constant $\alpha$. When $d_W$ or $d_Z$ is much larger than $d_\gamma$, these three-body decay channels can play an important role with $m_N < m_W$, which will reduce the branching ratio of $N \to \nu\gamma$. The Universal FeynRules Output (UFO) [49,50] of the neutrino dipole model is used, and fed to MadGraph5aMC@NLO -v2.6.7 [51] to calculate the width of three-body decay channels of HNL.

In Fig. 1, we present the branching ratio for $N$ decaying to a photon plus active neutrino

$$\mathrm{Br}(N \to \nu\gamma) \equiv \frac{\Gamma_{N\to\nu\gamma}}{\Gamma_{N\to\nu\gamma} + \Gamma_{N\to\nu Z} + \Gamma_{N\to W\ell} + \Gamma_{N\to 3\text{-body}}} \qquad (9)$$

as the function of $m_N$ and the ratio of $a = d_W/d_B$. From the curves in the $a - \mathrm{Br}(N \to \nu\gamma)$ plane, we can find a very conspicuous sharp valley, because there is a singularity in $d_Z$ and $d_W$ with $a = -2\cot\theta_w \sim -3.7$. Around this singularity point, the three-body decay channels of HNL via off-shell $W$ and $Z$ bosons can be sizable and even dominant when $m_N < M_W$. While the four scenarios listed in Table I are all away from the singularity point $a \sim -3.7$, thus the three-body decay channels can be safely ignored in our following calculations. From the curves in the $m_N - \mathrm{Br}(N \to \nu\gamma)$ plane, it can be seen that the branching ratio always decreases with the increment of $m_N$ when $m_N > M_W$. Since the width of three-body decay channels can be neglected compared with the two-body decays when $m_N > M_W$, $\mathrm{Br}(N \to \nu\gamma)$ tends to be $d_\gamma^2/(d_\gamma^2 + d_Z^2 + d_W^2) = (4 + 3a^2)/(2\cos\theta_w + a\sin\theta_w)^2$. For the heavy neutrino with $M_N \gg M_Z$, the branching ratio $\mathrm{Br}(N \to \nu\gamma)$ will reach its maximum near $a = 0$, then decreases with the increment of $a$, and finally tends to be that obtained in scenario II with $d_B = 0$.

## III. ELECTRON COLLIDER SIGNALS

In this section, we will investigate the Dirac sterile neutrino $N$ production via the dipole portal at high energy $e^+e^-$ colliders, such as LEP, and future CEPC. At electron colliders, HNL production will proceed from the process $e^+e^- \to N\bar{\nu}_k + \mathrm{H.c.}$ via either the $Z$ or $\gamma$ mediator in the $s$ channel depending on dipole portal couplings $d_Z^k$, $d_\gamma^k$ with $k = e, \mu, \tau$, or via the $W$ mediator in the $t$ channel depending on electron neutrino dipole portal coupling $d_W^e$ in Eq. (3), respectively. With the subsequent decay channel $N \to \nu\gamma$ in the detector, the signature of a single

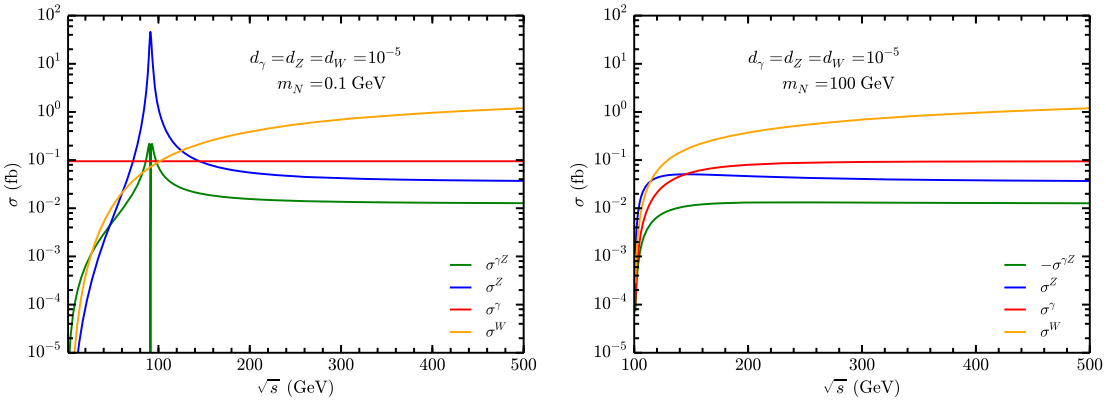


FIG. 2. The cross sections of the HNL associated with electron neutrino production as the function of c.m. energy $\sqrt{s}$ for $m_N = 0.1$ GeV (left) and $m_N = 100$ GeV (right) from $\gamma$, $Z$ and $W$ mediators with $d_\gamma = d_Z = d_W = 10^{-5}$. Since the cross section $\sigma^{\gamma Z}/(d_\gamma d_Z) < 0$ when $\sqrt{s} > M_Z$, its absolute value is shown.

photon final state with missing energy can be looked for at electron colliders. The total production cross section for $e^+e^- \to N\bar{\nu}$ after integrating over all angles from $\gamma$ and $Z$ mediators in the $s$ channel and the $W$ mediator in the $t$ channel can be respectively expressed as

$$\sigma^\gamma(e^+e^- \to N\bar{\nu}) = \frac{\alpha d_\gamma^2 (s - m_N^2)^2 (s + 2m_N^2)}{3s^3}, \quad (10)$$

$$\sigma^Z(e^+e^- \to N\bar{\nu}) = \frac{\alpha d_Z^2 (s - m_N^2)^2 (s + 2m_N^2)}{24 c_w^2 s_w^2 s(\Gamma_Z^2 M_Z^2 + (M_Z^2 - s)^2)} \times [(8s_w^2 - 4s_w + 1)], \quad (11)$$

$$\sigma^{\gamma Z}(e^+e^- \to N\bar{\nu}) = \frac{\alpha d_\gamma d_Z (s - m_N^2)^2 (s + 2m_N^2)}{6 c_w s_w s^2(\Gamma_Z^2 M_Z^2 + (M_Z^2 - s)^2)} \times [(-4s_w + 1)(M_Z^2 - s)], \quad (12)$$

$$\sigma^W(e^+e^- \to N\bar{\nu}_e) = \frac{\alpha (d_W^e)^2}{2 s_w^2 s} \left[ -2s - (2M_W^2 + s) \log \times \left( \frac{M_W^2}{-m_N^2 + M_W^2 + s} \right) + m_N^2 \left( \frac{M_W^2}{-m_N^2 + M_W^2 + s} + 1 \right) \right], \quad (13)$$

where $\sigma^{\gamma Z}$ denotes the interference term between $\gamma$ and $Z$ mediators in the $s$ channel, and the interference between the $s$ channel and the $t$ channel for electron neutrino vanished. One sees that at the low-energy electron colliders with $\sqrt{s} \ll M_Z$, the contribution from the $Z$ or the $W$ mediator can be neglected comparing with the one from the $\gamma$ mediator in the condition of $d_{Z,W}/d_\gamma \sim \mathcal{O}(1)$, which has been discussed in Ref. [43] at the low-energy electron colliders, such as BESIII, Belle II, and future STCF.

In Fig. 2, we present the cross sections of the HNL associated with electron neutrino production as the function of c.m. energy $\sqrt{s}$ for $m_N = 0.1$ GeV (left) and $m_N = 100$ GeV (right) from $\gamma$, $Z$, and $W$ mediators with $d_\gamma = d_Z = d_W = 10^{-5}$, separately. Note that, when $\sqrt{s} > M_Z$, there will be $\sigma^{\gamma Z}/(d_\gamma d_Z) < 0$, thus absolute values of $\sigma^{\gamma Z}$ are plotted in Fig. 2. We can see that the contribution from the $\gamma$ mediator $\sigma^\gamma$ has little to do with the c.m. energy when $m_N \ll \sqrt{s}$. The contribution $\sigma^Z$ from the $Z$ mediator for $m_N = 0.1$ GeV reaches its maximum when $\sqrt{s} = M_Z$ due to the $Z$ resonance. The contribution $\sigma^W$ from the $W$ mediator only appears in $N\bar{\nu}_e$ production, and can be ignored comparing with $\sigma^Z$ when $\sqrt{s}$ is around the $Z$ pole, while $\sigma^W$ always increases with the increment of $\sqrt{s}$, and will be dominant when $\sqrt{s} \gg M_Z$. Just thanks to the additional contribution $\sigma^W$ to electron neutrino production, the sensitivity on dipole coupling $d_\gamma^e$ will be different from $d_\gamma^\mu$ and $d_\gamma^\tau$ at electron colliders when $\sqrt{s} > M_Z$.

To make sure that there exists a visible photon in the final state, the subsequent decay of $N$ must occur inside the fiducial volume of the detector. The probability of the heavy neutrino to decay radiatively in the fiducial volume after traveling a distance $l$ from the primary vertex is given by

$$P_{\rm dec}(l) = (1 - e^{-l/l_{\rm dec}}) {\rm Br}(N \to \nu\gamma). \quad (14)$$

The decay length of $N$, $l_{\rm dec}$, scales as

$$l_{\rm dec} = c\tau\beta\gamma = \frac{4\pi}{d_\gamma^2 m_N^4} \sqrt{E_N^2 - m_N^2} \quad (15)$$

in the case of ${\rm Br}(N \to \nu\gamma) \simeq 1$, where $E_N$ is the energy of $N$, with $E_N = \frac{s + m_N^2}{2\sqrt{s}}$ in the process $e^+e^- \to N\bar{\nu}$.

Then, the production rates from new physics in the signal can be given as

$$\sigma^{\rm NP}(e^+e^- \to \gamma + {\rm INV}) = \sigma(e^+e^- \to N\nu) {\rm Br}(N \to \nu\gamma) \times \epsilon_{\rm cuts} \epsilon_{\rm det} P_{\rm dec}(l_D), \quad (16)$$

where $l_D$ is the detector length, $\epsilon_{\rm cuts}$ and $\epsilon_{\rm det}$ are the efficiencies of the kinematic cuts and detection for the final photon, respectively. Since $N$ is usually produced on shell and travels some distance before decaying, we employ the narrow width approximation to derive the kinematic information of the final state photon. The $1-\cos\theta$ distribution is used for the photon from $N$ decay, where $\theta$ is the photon angle in the rest frame of $N$ [52,53].

## IV. CONSTRAINTS FROM LEP

There are luxuriant analyses to search the monophoton signature at LEP, which can be used to set the constraints on dipole portal coupling to HNLs. In this section, we consider the single photon events with missing energy at the c.m. energies around the $Z$ pole at LEP1 and at larger c.m. energies above the $Z$ pole at LEP2. If the coupling between HNL and the $Z$ boson exists, there will be additional constraints from $Z$ decay, which has been measured accurately by LEP.

### A. LEP1

For the c.m. energies around the $Z$ pole at LEP1, the 95% confidence level (CL) upper limits on the integrated cross section for production of a single photon with $E_\gamma > E_{\rm min}$ and $|\cos\theta_\gamma| < 0.7$ are presented as the function of a specified minimum energy $E_{\rm min}$ by the OPAL collaboration [54]. We adopt the 95% CL limit of 0.15 pb on the cross section for production of a single photon with energy exceeding $E_{\rm min} = 23$ GeV in the $|\cos\theta_\gamma| < 0.7$ angular region to give the corresponding 95% CL limit on the dipole portal to HNLs. The corresponding upper bounds on the dipole coupling $d_\gamma$ are shown in Fig. 3 with green lines for the four scenarios listed in Table I, respectively. The overall detection efficiency of the photon is estimated to be 65.7% [54].

### B. LEP2

For larger c.m. energies above the $Z$ pole at LEP2, we use the DELPHI data of a single photon at $\sqrt{s} =$ 200–209 GeV (average $\sqrt{s} = 205.4$ GeV) in the angular region of $45° < \theta_\gamma < 135°$ and $0.06 < x_\gamma < 1.1$ with $x_\gamma = 2E_\gamma/\sqrt{s}$ [55]. The constraints on the dipole coupling can be obtained by performing a simple $\chi^2$ analysis with the function of

$$\chi^2 = \left(\frac{\sigma^{\rm SM} + \sigma^{N\nu} - \sigma^{\rm exp}}{\delta\sigma^{\rm exp}}\right)^2, \tag{17}$$

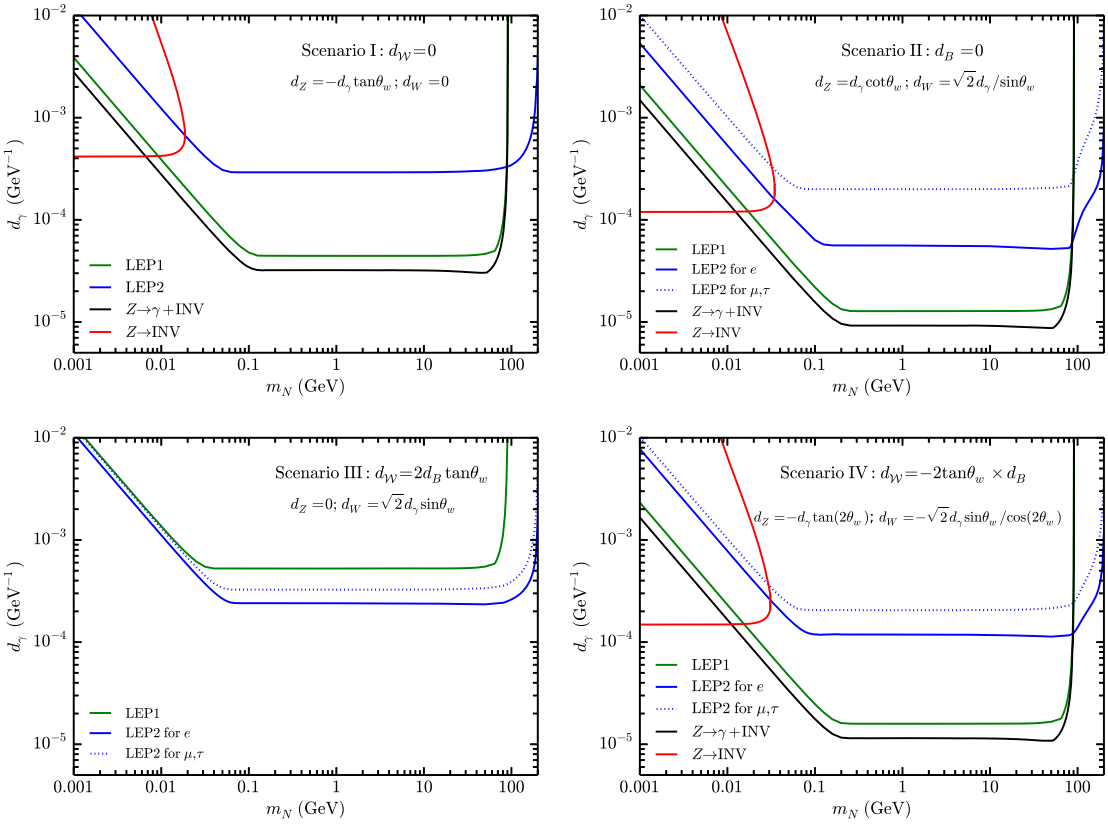


FIG. 3. The 95% CL upper bounds on the dipole portal coupling $d_\gamma$ under four assumptions listed in Table I from the monophoton searches at LEP1 [54] (green lines) and LEP2 [55] (blue solid lines for $d_\gamma^e$ and blue dotted lines for $d_\gamma^{\mu,\tau}$), the decay $Z \to \gamma +$ invisible [56] (black lines) and $Z$ invisible decay [57] (red lines), respectively.

with $\sigma^{\rm SM} = 1.61$ pb, $\sigma^{\rm exp} = 1.50$ pb, and $\delta\sigma^{\rm exp} = 0.11$ pb from Ref. [55]. Estimated from the Monte Carlo cross sections and the expected numbers of events, the overall detection efficiency of the photon is set to be 65%. The 95% CL upper limits on the dipole coupling $d_\gamma$ are shown in Fig. 3 with blue lines for the four scenarios.

### C. Z decay

Negative evidence for the single photon with a missing energy signal at L3 detector of LEP1 [56] set an upper limit at the 95% CL lying in the range of about $(3.2 \sim 1.1) \times 10^{-6}$ on the branching ratio for $Z$ decaying to invisible particles and a photon with energy greater that $E_{\rm min}$ in the range of $(15 \sim 40)$ GeV. The measurable decay width $\Gamma_{Z\to\gamma+\text{invisible}}$ at LEP from dipole portal to HNLs can be expressed as

$$\Gamma^{\rm NP}_{Z\to\gamma+\text{invisible}} = (\Gamma_{Z\to N\bar{\nu}} + \Gamma_{Z\to\bar{N}\nu})\text{Br}(N\to\nu\gamma) \times \epsilon_{\rm cuts}(1 - P_{\rm dec}(l_D)). \quad (18)$$

Here the decay width of $Z \to N\bar{\nu}$ or $Z \to \bar{N}\nu$ can be given as

$$\Gamma_{Z\to N\bar{\nu}} = \Gamma_{Z\to\bar{N}\nu} = \frac{d_Z^2(M_Z^2 - m_N^2)^2(2m_N^2 + M_Z^2)}{12\pi m_Z^3}\Theta \times (m_Z > M_N), \quad (19)$$

and $P_{\rm dec}(l_D)$ denotes the probability of heavy neutrino $N$ to decay radiatively out of the detector at LEP with the detector length $l_D = 1$ m; $\epsilon_{\rm cuts}$ is the efficiency of the kinematic cuts with $E_\gamma > E_{\rm min}$ for the final photon. We use the 95% CL upper limit of $3.2 \times 10^{-6}$ on the branching ratio $\text{Br}(Z \to \gamma + \text{invisible})$ with $E_\gamma > 15$ GeV to provide the corresponding 95% CL constraint on dipole portal coupling $d_\gamma$, which is presented in Fig. 3 with black lines.

Besides, $N$ decaying out of the detector will contribute to the $Z$-boson invisible decay as

$$\Gamma^{\rm NP}_{Z\to\text{invisible}} = (\Gamma_{Z\to N\bar{\nu}} + \Gamma_{Z\to\bar{N}\nu})P_{\rm dec}(l_D). \quad (20)$$

The total width of the $Z$ boson has been measured accurately by the LEP experiments which place a strong bound on new physics contributions $\Gamma^{\rm NP}_{Z\to\text{invisible}} < 2.0$ MeV at 95% CL [57]. The 95% CL upper limits from $Z$ invisible decay on the dipole coupling are given in Fig. 3 with red lines.

### D. Results

One sees that the constraints from monophoton searches at LEP1 and LEP2, and from $Z$ decaying into invisible particles associated with a photon, have a characteristic "U" shape. The right boundary of the "U" shape region for lager $m_N$ is controlled by the kinematic reach, and in the case of the LEP2 extends beyond 100 GeV. The left boundary of the excluded "U" shape region for small $m_N$ is controlled by the lifetime of $N$. Since smaller $m_N$ leads to the longer lifetime of $N$, $N$ will more likely decay out of the detector with the loss of the $\gamma$ signal. The $Z$ invisible decay can provide complementary constraints for the HNLs with small mass.

Note that because of the additional contribution from the $W$ mediator diagram in the $t$ channel for $N\nu_e$ production, the constraints on $d_\gamma^e$ (blue solid lines) will be stricter than $d_\gamma^{\mu,\tau}$ (blue dotted lines) from monophoton searches at LEP2 with $\sqrt{s} > M_Z$ when $d_W \neq 0$, which can be seen in scenarios II, III, and IV. In scenarios I, II, and IV with $d_Z \neq 0$, there will be additional constraints from $Z$ decay. The measurements of $Z$ decay will derive the same sensitivity for all three lepton flavors, so almost do the monophoton searches at LEP1, since $\sigma^W$ can be ignored comparing with $\sigma^Z$ around the $Z$ pole.

Since LEP1 with $\sqrt{s} \simeq M_Z$ can provide very competitive production rates of HNL due to the $Z$ resonance from the $Z$ mediator in the $s$ channel when $d_Z \neq 0$, the sensitivities on the dipole portal coupling $d_\gamma$ are much better at LEP1, which can be about 1 order of magnitude than the ones at LEP2 with $m_N \lesssim 90$ GeV in scenarios I, II, and IV. While in scenario III with $d_Z = 0$, LEP2 always gives leading constraints in all the plotted mass region. Though there is no $Z$-resonance enhancement in scenario III with $d_Z = 0$ at LEP1, the limits for different lepton flavors are still almost the same since $\sigma^\gamma$ is more dominant than $\sigma^W$ around the $Z$ pole. The constraints from the measurement of the branching ratio for $Z \to \gamma +$ invisible are always found to be more stringent than the ones from monophoton searches at LEP1 in the scenarios with $d_Z \neq 0$.

In Fig. 4, we present the production rate for the sterile neutrino associated with the active neutrino at electron colliders with $\sqrt{s} = M_Z$ (left), and the branching ratio of $Z \to \gamma +$ invisible (right), as the function of $a = d_W/d_B$, which are all labeled with a red line, respectively. Here we set $m_N = 10$ GeV and $d_\gamma = 10^{-7}$. Since there is a singularity in $d_Z$ and $d_W$ at $a = -2\cot\theta_w \sim -3.7$, the production rate of $N\nu$ and the branching ratio of $Z \to \gamma +$ invisible will increase when $a < -2\cot\theta_w$ with the increment of $a$, then decrease until $a = 2\tan\theta_w \sim 1.1$. With $a = 2\tan\theta_w$, the dipole coupling with the $Z$ boson $d_Z$ becomes zero, the production rate reaches its minimum and the branching ratio goes to zero. The corresponding 95% CL upper limits on dipole coupling $d_\gamma$ as the function of $a$ from the monophoton searches (left) and the measurement of $Z \to \gamma +$ invisible (right) at LEP1 are also shown in Fig. 4 with black solid lines, respectively. In the case of $a > 0$, the upper bounds on $d_\gamma$ lie in the range of $(2.0 \times 10^{-5}, 4.5 \times 10^{-4})$ from monophoton searches at LEP1. Besides the region very near $a = 2\tan\theta_w$ where $d_Z$ is close to zero, the measurement of $Z$ decaying into photon plus invisible particles can provide a stricter constraint than monophoton searches at LEP1.

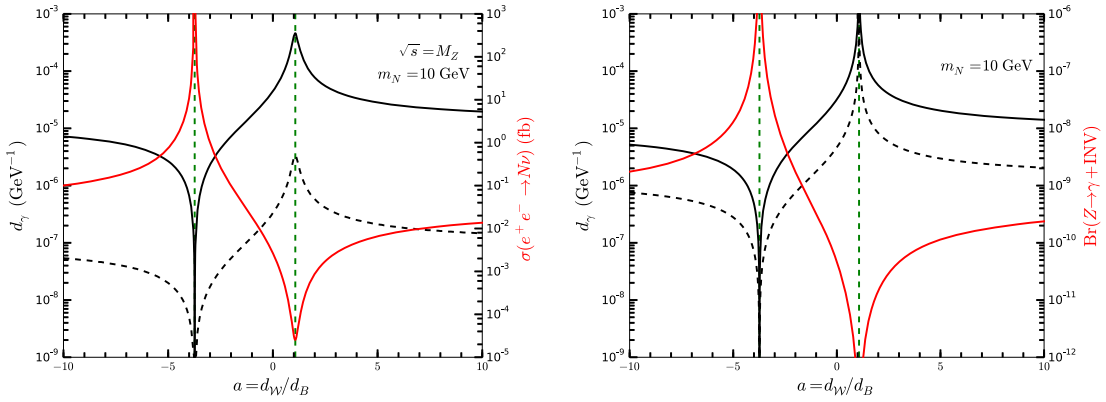


FIG. 4. Left: the production rates for the process $e^+e^- \to N\bar{\nu}$ (red line) with $m_N = 10$ GeV, $d_\gamma = 10^{-7}$, and $\sqrt{s} = M_Z$, and the 95% CL upper limits on the neutrino dipole portal coupling to HNLs $d_\gamma$ as the function of the ratio $a = d_W/d_B$ with the c.m. energy on the $Z$ pole using the monophoton searches by the OPAL collaboration at LEP1 [54] (black solid line) and future CEPC (black dashed line) with the luminosity of 100 ab$^{-1}$. Right: the branching ratio for $Z$ decaying into invisible particles and a photon Br($Z \to \gamma +$ invisible) (red line) with $m_N = 10$ GeV and $d_\gamma = 10^{-7}$, and the constraints on $d_\gamma$ as the function of the ratio $a = d_W/d_B$ assuming Br($Z \to \gamma +$ invisible) $= 10^{-7}$ in the future (black dashed line) and 95% CL upper upper limit of Br($Z \to \gamma +$ invisible) $= 3.2 \times 10^{-6}$ with $E_\gamma > 15$ GeV from LEP (black solid line).

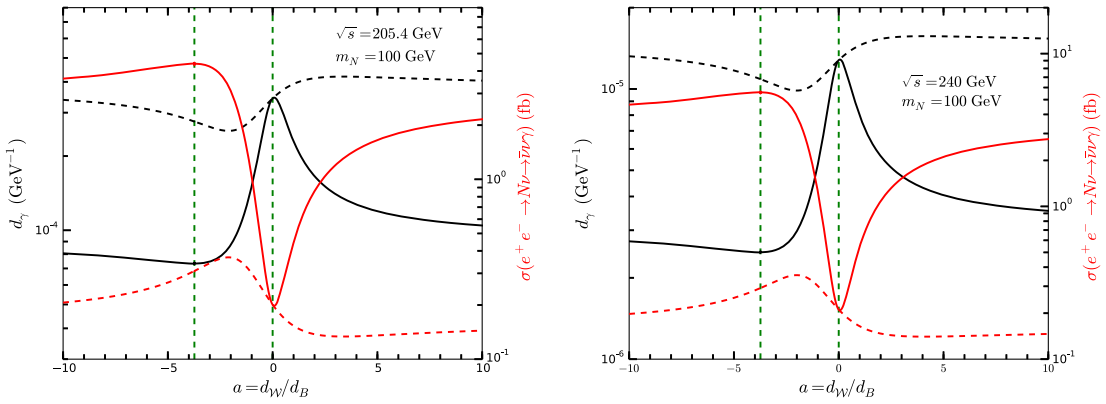


FIG. 5. The production rates for the processes $e^+e^- \to N\nu_e \to \nu_e\bar{\nu}_e\gamma$ (red solid line) and $e^+e^- \to N\nu_{\mu,\tau} \to \nu_{\mu,\tau}\bar{\nu}_{\mu,\tau}\gamma$ (red dashed line) with $m_N = 100$ GeV, $d_\gamma = 10^{-5}$, and $\sqrt{s} = 205.4$ GeV, and the 95% CL upper limits on the neutrino dipole portal couplings $d_\gamma^e$ (black solid line) and $d_\gamma^{\mu,\tau}$ (black dashed line) as the function of the ratio $a = d_W/d_B$ using the monophoton searches by the OPAL collaboration at LEP2 [54] (left) and future CEPC in $H$ mode with the luminosity of 20 ab$^{-1}$ (right).

The graph on the left of Fig. 5 shows the production rates of the processes $e^+e^- \to N\nu_e \to \nu_e\bar{\nu}_e\gamma$ (red solid line) and $e^+e^- \to N\nu_{\mu,\tau} \to \nu_{\mu,\tau}\bar{\nu}_{\mu,\tau}\gamma$ (red dashed line) as the function of $a$ with $m_N = 100$ GeV and $d_\gamma = 10^{-5}$ at LEP2 with $\sqrt{s} = 205.4$ GeV. The kinematic cuts and the detection efficiency for the final photon in DELPHI data [55] are also considered. Interestingly, the cross sections of the monophoton due to $N$ production for $m_N = 100$ GeV at the electron collider are observed to change not too much around $a = -2\cot\theta_w$, not as drastically as in Fig. 4 for $m_N = 10$ GeV. This is because when $m_N > M_Z$, the opening of decay channel $N \to \ell W$ and $N \to \nu Z$ will reduce the branching ratio of $N \to \nu\gamma$, which is inversely proportional to $(d_Z^2 + d_W^2)$ and thereby offset the dependence of the production rate for monophoton on the couplings $d_Z$ or $d_W$. From the difference between the production rates of $\nu_e\bar{\nu}_e\gamma$ and $\nu_{\mu,\tau}\bar{\nu}_{\mu,\tau}\gamma$ in Fig. 5, one can find the additional contribution from the $W$-mediator diagram in the $t$ channel for the production of $N$. The corresponding 95% CL upper limits on the dipole portal couplings $d_\gamma^e$ (black solid line) and $d_\gamma^{\mu,\tau}$ (black dashed line) for $m_N = 100$ GeV using DELPHI data of the monophoton search [55] at LEP2 are also shown in the graph on the left of Fig. 5. For $|a| \leq 10$, the upper limits on the dipole portal couplings to HNL with mass of 100 GeV, $d_\gamma^e$ and $d_\gamma^{\mu,\tau}$, lie in the range of $(7.1 \times 10^{-5}, 3.5 \times 10^{-4})$ and $(2.5 \times 10^{-4}, 4.1 \times 10^{-4})$ from monophoton searches at LEP2, respectively. When $a = 0$ $(d_W = 0)$, the upper limit on $d_\gamma^e$ reaches its maximum.

## V. CONSTRAINTS FROM CEPC

In the following, we will investigate the sensitivity on the dipole portal coupling to HNLs at the future electron collider CEPC [47,48]. The CEPC, proposed by the Chinese high energy physics community in 2012, is designed to run primarily at a c.m. energy of 240 GeV as a Higgs factory ($H$ mode) with a total luminosity of 20 ab$^{-1}$ for ten years running [58]. In addition, on the $Z$ pole as a $Z$ factory ($Z$ mode), it will also be operated with a total luminosity of 100 ab$^{-1}$ for two years, perform a precise $WW$ threshold scan ($WW$ mode) with a total luminosity of $\sim$6 ab$^{-1}$ for one year running at $\sqrt{s} \sim 160$ GeV, and will be upgraded to a c.m. energy of 360 GeV, close to the $t\bar{t}$ threshold ($t\bar{t}$ mode) with a total luminosity of $\sim$1 ab$^{-1}$ for five years [58].

In the search for a monophoton signature at CEPC, the backgrounds can be classified into two categories: the irreducible background and the reducible background. The irreducible background arises from the neutrino production associated with one photon in SM $e^+e^- \to \nu\bar{\nu}\gamma$. The reducible background comes from any SM process with a single photon in the final state with all other visible particles undetected due to limitations of the detector acceptance. Such as the radiative Bhabha scattering, $e^+e^- \to e^+e^-\gamma$ should be considered carefully, which has a huge cross section and can mimic the signal if both the final state electrons and positrons escape undetected, for example, through the beam pipes [59,60].

For the monophoton signature at CEPC, we use the cuts for the final detected photon following the CEPC conceptual design report [48]: $|z_\gamma| < 0.99$ and $E_\gamma > 0.1$ GeV (hereafter the "preselection cut"). Because of the SM $Z$ boson, the irreducible background from the SM neutrino pair production $e^+e^- \to \nu\bar{\nu}\gamma$ exhibits a resonance in the monophoton energy spectrum which exhibits a peak at the photon energy $E_\gamma^Z = (s - M_Z^2)/2\sqrt{s}$ with a full-width-at-half maximum as $\Gamma_\gamma^Z = M_Z\Gamma_Z/\sqrt{s}$. To suppress the irreducible background contribution, we will veto the events within $E_\gamma \in (E_\gamma^Z \pm 5\Gamma_\gamma^Z)$ in the monophoton energy spectrum [61] (hereafter the "Z resonance veto cut"). We apply the cut,

$$E_\gamma > E_\gamma^m(\theta_\gamma) = \frac{\sqrt{s}}{(1 + \sin\theta_\gamma/\sin\theta_b)}, \tag{21}$$

on the final state photon to remove the main reducible background from the processes $e^+e^- \to e^+e^-\gamma$ and $e^+e^- \to \gamma\gamma\gamma$ following Ref. [61], where $\theta_b$ denotes the angle at the boundary of the subdetectors with $\cos\theta_b = 0.99$. We will collectively refer to preselection cut, Z resonance veto cut and cut of (21) in the list as the "basic cuts" hereafter.

In Fig. 6, we present the normalized transverse momentum distribution of the final state photon due to the background and the signal from the sterile neutrino after the "advanced cut" at CEPC in $Z$ mode and $H$ mode, respectively. It can be seen that, compared to the background, the typical feature of the signal is that the final state photon is distributed in the large transverse momentum regions, especially for larger $m_N$. Thus, in order to improve the sensitivity, we impose the transverse momentum cut in addition to the basic cuts for the final state photon with $p_T^\gamma > 35$ GeV in the $Z$ mode, $p_T^\gamma > 35$ GeV in the $Z$ mode, $p_T^\gamma > 65$ GeV in the $WW$ mode, $p_T^\gamma > 100$ GeV in the $H$ mode, and $p_T^\gamma > 160$ GeV in the $t\bar{t}$ mode, respectively. We collect the $p_T^\gamma$ cut and the "basic detector cuts" as the "advanced cuts."

The simple criteria $S^2/B = 2.71$ is used to probe the 95% CL upper bounds on the neutrino dipole portal couplings $d_\gamma$ at CEPC, which are shown in Fig. 7. Here we consider four scenarios with assumptions as $d_{\mathcal{W}} = 0$, $d_B = 0$, and $d_{\mathcal{W}} = \pm 2\tan\theta_w d_B$, respectively, which are listed in Table. I. The limits are calculated based on the total luminosity of 20 ab$^{-1}$ data in the $H$ mode (orange lines), 6 ab$^{-1}$ in the $WW$ mode (blue lines), 100 ab$^{-1}$ in the $Z$ mode (green lines), and 1 ab$^{-1}$ in the $t\bar{t}$ mode (red lines).

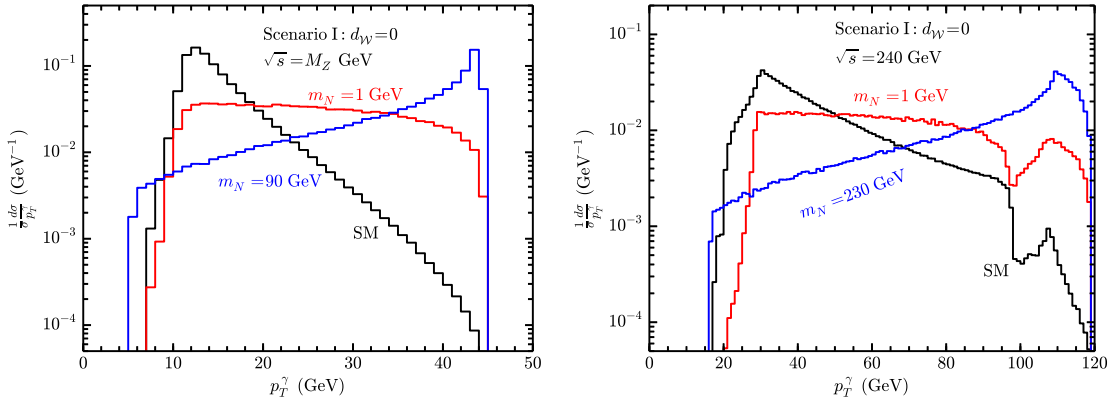


FIG. 6. The normalized transverse momentum distribution of the final photon due to the background and the signal from sterile neutrino after the advanced cut at CEPC in the $Z$ mode (left) and the $H$ mode (right). For the signal from sterile neutrino, we consider $m_N = 1$ GeV, and 90 GeV in the $Z$ mode, and $m_N = 1$ GeV, and 230 GeV in the $H$ mode.

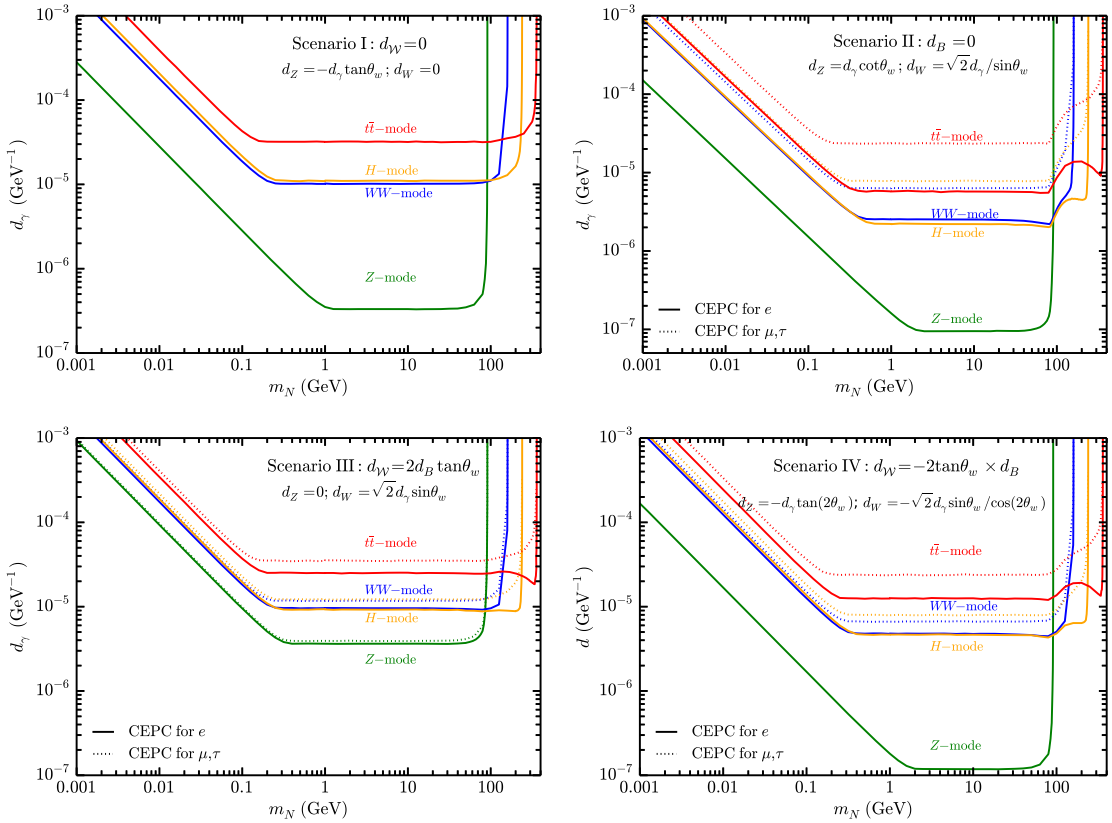


FIG. 7. The expected 95% CL upper limits on the electron-neutrino $d_\gamma^e$ (solid lines), and muon- or tau-neutrino $d_\gamma^{\mu,\tau}$ (dotted lines) dipole portal coupling to HNLs under four assumptions listed in Table I at CEPC in the $Z$ mode with 100 ab$^{-1}$ luminosity (green lines), in the $H$ mode with 20 ab$^{-1}$ luminosity (black lines), in the $WW$ mode with 6 ab$^{-1}$ luminosity (blue lines), and in the $t\bar{t}$ mode with 1 ab$^{-1}$ luminosity (red lines), respectively.

There is an additional contribution from the $W$ boson, therefore the constraints on $d_\gamma^e$ (plotted with solid lines) are always more stringent than $d_\gamma^{\mu,\tau}$ (plotted with dotted lines) except in scenario I with $d_W=0$ where the sensitivities on all three lepton flavors are the same. In the $Z$ mode at CEPC, the constraints on $d_\gamma$ with different lepton flavor are almost the same, because the additional contribution $t$ channel for the electron can be neglected compared to the $s$ channel due to the $Z$ resonance when $d_Z\neq 0$.

One can see that the $Z$ mode has the best sensitivity in all four scenarios for the HNL with small mass. Especially in scenarios I, II, and IV with $d_Z\neq 0$, the upper limits of $d_\gamma^e$ probed by the $Z$ mode are stronger than ones by the other three running modes at CEPC beyond 1 order of magnitude in the mass region of about $(1\sim 50)$ GeV. What is more, in scenarios II and IV, the $Z$ mode can give about 2 orders of magnitude of improvement over the other three running modes at CEPC in the sensitivity on $d_\gamma^{\mu,\tau}$. This is because the $Z$ resonance with $\sqrt{s}\simeq M_Z$ can significantly improve the production rate for HNLs at electron colliders.

In Fig. 4, we show the 95% CL upper limits on dipole coupling $d_\gamma$ with $m_N=10$ GeV as the function of $a$ in the $Z$ mode at CEPC via the monophoton searches, which is plotted with a black dashed line. One sees that the curve has similar behavior with the one from LEP1. The upper bounds on $d_\gamma$ with $a>0$ lie in the range of $(1.5\times 10^{-7}, 3.3\times 10^{-6})$, which is about 2 orders of magnitude lower than LEP1. We also present a projection for $d_\gamma$ as the function of $a$ with an imaginary limit on the branching ratio of $10^{-7}$ in the future for the HNL with mass of 10 GeV at 95% CL on the right of Fig. 4 with a black dashed line.

The graph on the right of Fig. 5 shows the production rates of the processes $e^+e^-\to N\nu_e\to\nu_e\bar{\nu}_e\gamma$ (red solid line) and $e^+e^-\to N\nu_{\mu,\tau}\to\nu_{\mu,\tau}\bar{\nu}_{\mu,\tau}\gamma$ (red dashed line) as the function of $a$ with $m_N=100$ GeV and $d_\gamma=10^{-5}$ at CEPC with $\sqrt{s}=240$ GeV in the $H$ mode. The corresponding 95% CL upper limits on the dipole portal couplings $d_\gamma^e$ (black solid line) and $d_\gamma^{\mu,\tau}$ (black dashed line) for $m_N=100$ GeV with the luminosity of 20 ab$^{-1}$. With $|a|\leq 10$ and $m_N=100$ GeV, the upper limits on the dipole portal couplings to HNL, $d_\gamma^e$ and $d_\gamma^{\mu,\tau}$, lie in the range of $(2.5\times 10^{-6}, 1.3\times 10^{-5})$ and $(9.9\times 10^{-6}, 1.6\times 10^{-5})$ from monophoton searches at future CEPC in the $H$ mode, respectively.

## VI. DISCUSSION AND CONCLUSION

The landscape of current constraints on active-sterile neutrino transition magnetic moments $d_\gamma^k$ with $k = e, \mu, \tau$, which are from terrestrial experiments such as Borexino [25], Xenon-1T [25], CHARM-II [21], MiniBooNE [24], LSND [24], NOMAD [24,62], and DONUT [63], and astrophysics supernovae SN 1987A [24], are summarized in Fig. 8 with gray shaded regions, respectively. These constraints basically do not depend on the ratio $a = d_\mathcal{W}/d_B$, since the typical scattering energies are far less than the electroweak scale. It is noted that the constraints from XENON-1T, Borexino [25], and SN 1987A [24] are flavor universal.

The blue shaded regions in Fig. 8 present the sensitivities on $d_\gamma$ at LEP in four scenarios listed in Table I, which are the combination of the best constraints shown in Fig. 3 using the monophoton data by the OPAL collaboration at LEP1 [54] and by the DELPHI collaboration at LEP2 [55], and the measurement of $Z$ decay [56,57]. The combination of the best constraints from four running modes at CEPC in Fig. 7 are also shown in Fig. 8 with red lines. It can be found that the constraints from $Z$ invisible decay measured at LEP are already excluded by Xenon-1T. The constraints on transition magnetic moments involving three SM active neutrinos ($\nu_{e,\mu,\tau}$) are the same from the measurement of $Z$ decay, while the constraints from the monophoton searches at LEP and future CEPC are in principle different on $d_\gamma^e$ and on $d_\gamma^{\mu,\tau}$ when $a \neq 0$ ($d_\mathcal{W} \neq 0$), because there will be additional contributions from the $W$ mediator.

For $d_\gamma^e$, beside the flavor-universal constraints from XENON-1T, Borexino [25], and SN 1987A [24], there are also complementary limits from LSND [24] with $m_N \lesssim 0.07$ GeV. For heavier $N$ only coupling with $\nu_e$, LEP can explore the previously unconstrained parameter region, and will be greatly improved by CEPC. In scenario III, with $d_Z = 0$, the contribution from the $Z$ boson vanishes, leading to weakest limits on $d_\gamma^e$ than the other three scenarios which can be down to about $3.3 \times 10^{-4}$ at LEP and $3.6 \times 10^{-6}$ at CEPC. In scenario II, with $d_B = 0$, CEPC can probe the limit on $d_\gamma^e$ down to about $9.5 \times 10^{-8}$, which is more than 2 orders of magnitude stronger than

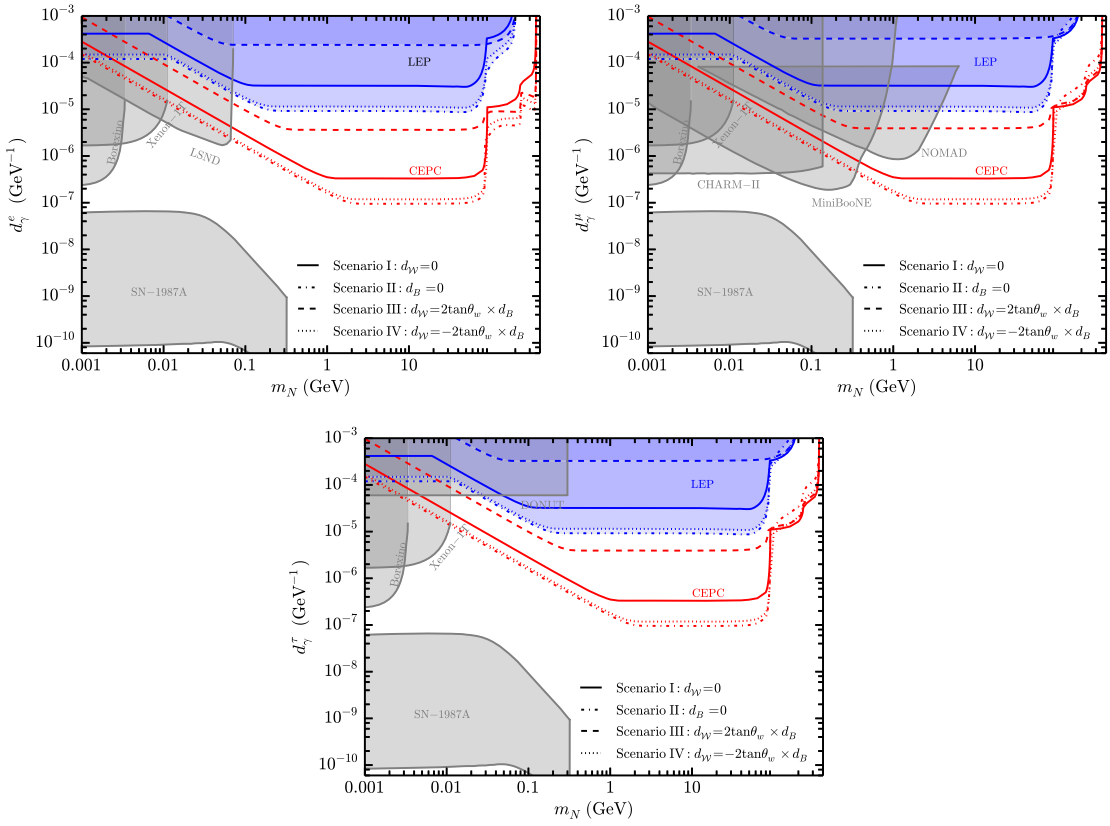


FIG. 8. The expected 95% CL exclusion limits on active-sterile neutrino transition magnetic moment $d_\gamma$ in four scenarios listed in Table I at LEP (blue shaded regions), which are the combination of the best constraints shown in Fig. 3 using the monophoton data by the OPAL collaboration at LEP1 [54] and by the DELPHI collaboration at LEP2 [55], and the measurement of $Z$ decay [56,57], and at CEPC (red lines), which are the combination of the best constraints from four running modes at CEPC in Fig. 7, for three lepton flavor respectively. The landscape of current leading constraints is also shown with shaded regions, exploiting from Borexino [25], Xenon1T [25], LEP [24], and SN-1987A [24], which are relevant for all three SM neutrinos; LSND [24] only for $d_\gamma^e$; CHARM-II [21], MiniBooNE [24], and NOMAD [24,62] only for $d_\gamma^\mu$; DONUT [63] only for $d_\gamma^\tau$.

LEP, with the limit down to about $1.3 \times 10^{-5}$ from the measurement of $\mathrm{Br}(Z \to \gamma + \text{invisible})$.

For $d_\gamma^\mu$, there are terrestrial constraints from CHARM-II [21], MiniBooNE, and NOMAD [24]. In scenario III, the best limit on $d_\gamma^\mu$ at LEP is from the monophoton searches by the DELPHI collaboration at LEP2 [55] in the plotted region, which is weaker than the one on $d_\gamma^e$ due to the absence of the $W$-exchanging channel, while it still can touch the unexplored parameter region when $m_N \gtrsim 1$ GeV. In the other three scenarios with $d_Z \neq 0$, the limits on $d_\gamma^\mu$ with $m_N \lesssim 90$ GeV shown in Fig. 8 are from the $Z$ decay measurements at LEP, thus they are the same with $d_\gamma^e$, which are ahead of the current limits from NOMAD [24] with $m_N$ larger than 5.0, 3.6, and 3.9 GeV in scenarios I, II, and IV, respectively. The expected limits from the monophoton searches at CEPC are complementary to the current limits when $m_N \gtrsim 3.5$ GeV in scenario III and $m_N \gtrsim 0.4$ GeV in the other three scenarios.

On $d_\gamma^\tau$, there is an upper 90% CL limit given by DONUT [63] of $5.8 \times 10^{-5}$ GeV$^{-1}$ for $m_N < 0.3$ GeV. The constraints on $d_\gamma^\tau$ from LEP and CEPC are the same with $d_\gamma^\mu$. The monophoton searches at LEP2 can provide complementary constraints to DONUT on $d_\gamma^\tau$ when $m_N > 0.3$ GeV in scenario III with $d_Z = 0$. In other scenarios with $d_Z \neq 0$, the measurement of $Z \to \gamma +$ invisible at LEP can provide leading sensitivity on $d_\gamma^\tau$ with $m_N \gtrsim 0.05(0.03)$ GeV in scenario I (II/IV), respectively. The monophoton searches at CEPC can fill a huge unconstrained void of the $d_\gamma^\tau - m_N$ parameter space when $m_N \gtrsim 0.2$ GeV.

## ACKNOWLEDGMENTS

This work was supported in part by the National Natural Science Foundation of China (Grants No. 12205153 and No. 11805001) and the 2021 Jiangsu Shuangchuang (Mass Innovation and Entrepreneurship) Talent Program (No. JSSCBS20210213).

[1] M. Sajjad Athar *et al.*, Status and perspectives of neutrino physics, Prog. Part. Nucl. Phys. **124**, 103947 (2022).
[2] R. L. Workman *et al.* (Particle Data Group), Review of particle physics, Prog. Theor. Exp. Phys. **2022**, 083C01 (2022).
[3] S. Balaji, M. Ramirez-Quezada, and Y.-L. Zhou, *CP* violation and circular polarisation in neutrino radiative decay, J. High Energy Phys. 04 (2020) 178.
[4] S. Balaji, M. Ramirez-Quezada, and Y.-L. Zhou, *CP* violation in neutral lepton transition dipole moment, J. High Energy Phys. 12 (2020) 090.
[5] F. Delgado, L. Duarte, J. Jones-Perez, C. Manrique-Chavil, and S. Peña, Assessment of the dimension-5 seesaw portal and impact of exotic Higgs decays on non-pointing photon searches, J. High Energy Phys. 09 (2022) 079.
[6] D. Barducci, E. Bertuzzo, M. Taoso, and C. Toni, Probing right-handed neutrinos dipole operators, J. High Energy Phys. 03 (2023) 239.
[7] J.-N. Ding, Q. Qin, and F.-S. Yu, Heavy neutrino searches at future $Z$-factories, Eur. Phys. J. C **79**, 766 (2019).
[8] Y.-F. Shen, J.-N. Ding, and Q. Qin, Monojet search for heavy neutrinos at future Z-factories, Eur. Phys. J. C **82**, 398 (2022).
[9] F. F. Deppisch, W. Liu, and M. Mitra, Long-lived heavy neutrinos from Higgs decays, J. High Energy Phys. 08 (2018) 181.
[10] F. Deppisch, S. Kulkarni, and W. Liu, Heavy neutrino production via $Z'$ at the lifetime frontier, Phys. Rev. D **100**, 035005 (2019).
[11] W. Liu, S. Kulkarni, and F. F. Deppisch, Heavy neutrinos at the FCC-hh in the $U(1)_{B-L}$ model, Phys. Rev. D **105**, 095043 (2022).
[12] W. Liu, K.-P. Xie, and Z. Yi, Testing leptogenesis at the LHC and future muon colliders: A Z' scenario, Phys. Rev. D **105**, 095034 (2022).
[13] W. Liu, J. Li, J. Li, and H. Sun, Testing the seesaw mechanisms via displaced right-handed neutrinos from a light scalar at the HL-LHC, Phys. Rev. D **106**, 015019 (2022).
[14] M. Dvornikov and A. Studenikin, Electric charge and magnetic moment of massive neutrino, Phys. Rev. D **69**, 073001 (2004).
[15] R. E. Shrock, Electromagnetic properties and decays of Dirac and Majorana neutrinos in a general class of gauge theories, Nucl. Phys. **B206**, 359 (1982).
[16] P. B. Pal and L. Wolfenstein, Radiative decays of massive neutrinos, Phys. Rev. D **25**, 766 (1982).
[17] K. Fujikawa and R. Shrock, The Magnetic Moment of a Massive Neutrino and Neutrino Spin Rotation, Phys. Rev. Lett. **45**, 963 (1980).
[18] A. Aparici, K. Kim, A. Santamaria, and J. Wudka, Right-handed neutrino magnetic moments, Phys. Rev. D **80**, 013010 (2009).
[19] C. Giunti and A. Studenikin, Neutrino electromagnetic interactions: A window to new physics, Rev. Mod. Phys. **87**, 531 (2015).
[20] A. Aparici, Exotic properties of neutrinos using effective Lagrangians and specific models, arXiv:1312.0554.
[21] P. Coloma, P. A. N. Machado, I. Martinez-Soler, and I. M. Shoemaker, Double-Cascade Events from New Physics in Icecube, Phys. Rev. Lett. **119**, 201804 (2017).
[22] K. N. Abazajian, Sterile neutrinos in cosmology, Phys. Rep. **711–712**, 1 (2017).

[23] I. M. Shoemaker and J. Wyenberg, Direct detection experiments at the neutrino dipole portal frontier, Phys. Rev. D **99**, 075010 (2019).

[24] G. Magill, R. Plestid, M. Pospelov, and Y.-D. Tsai, Dipole portal to heavy neutral leptons, Phys. Rev. D **98**, 115015 (2018).

[25] V. Brdar, A. Greljo, J. Kopp, and T. Opferkuch, The neutrino magnetic moment portal: Cosmology, astrophysics, and direct detection, J. Cosmol. Astropart. Phys. 01 (2021) 039.

[26] R. Plestid, Luminous solar neutrinos I: Dipole portals, Phys. Rev. D **104**, 075027 (2021).

[27] K. Jodłowski and S. Trojanowski, Neutrino beam-dump experiment with FASER at the LHC, J. High Energy Phys. 05 (2021) 191.

[28] T. Schwetz, A. Zhou, and J.-Y. Zhu, Constraining active-sterile neutrino transition magnetic moments at DUNE near and far detectors, J. High Energy Phys. 07 (2021) 200.

[29] A. Ismail, S. Jana, and R. M. Abraham, Neutrino upscattering via the dipole portal at forward LHC detectors, Phys. Rev. D **105**, 055008 (2022).

[30] O. G. Miranda, D. K. Papoulias, O. Sanders, M. Tórtola, and J. W. F. Valle, Low-energy probes of sterile neutrino transition magnetic moments, J. High Energy Phys. 12 (2021) 191.

[31] A. Dasgupta, S. K. Kang, and J. E. Kim, Probing neutrino dipole portal at COHERENT experiment, J. High Energy Phys. 11 (2021) 120.

[32] M. Atkinson, P. Coloma, I. Martinez-Soler, N. Rocco, and I. M. Shoemaker, Heavy neutrino searches through double-bang events at Super-Kamiokande, DUNE, and Hyper-Kamiokande, J. High Energy Phys. 04 (2022) 174.

[33] N. W. Kamp, M. Hostert, A. Schneider, S. Vergani, C. A. Argüelles, J. M. Conrad, M. H. Shaevitz, and M. A. Uchida, Dipole-coupled neutrissimo explanations of the MiniBooNE excess including constraints from MINERvA data, Phys. Rev. D **107**, 055009 (2023).

[34] R. A. Gustafson, R. Plestid, and I. M. Shoemaker, Neutrino portals, terrestrial upscattering, and atmospheric neutrinos, Phys. Rev. D **106**, 095037 (2022).

[35] G.-y. Huang, S. Jana, M. Lindner, and W. Rodejohann, Probing heavy sterile neutrinos at ultrahigh energy neutrino telescopes via the dipole portal, Phys. Lett. B **840**, 137842 (2023).

[36] Y.-F. Li and S.-y. Xia, Probing neutrino magnetic moments and the Xenon1T excess with coherent elastic solar neutrino scattering, Phys. Rev. D **106**, 095022 (2022).

[37] M. A. Acero *et al.*, White paper on light sterile neutrino searches and related phenomenology, arXiv:2203.07323.

[38] J. L. Feng *et al.*, The forward physics facility at the high-luminosity LHC, J. Phys. G **50**, 030501 (2023).

[39] C. Hati, P. Bolton, F. F. Deppisch, K. Fridell, J. Harz, and S. Kulkarni, Distinguishing Dirac vs Majorana neutrinos at CE$\nu$NS experiments, Proc. Sci. EPS-HEP2021 (**2022**) 225.

[40] V. Mathur, I. M. Shoemaker, and Z. Tabrizi, Using DUNE to shed light on the electromagnetic properties of neutrinos, J. High Energy Phys. 10 (2022) 041.

[41] P. D. Bolton, F. F. Deppisch, K. Fridell, J. Harz, C. Hati, and S. Kulkarni, Probing active-sterile neutrino transition magnetic moments with photon emission from CE$\nu$NS, Phys. Rev. D **106**, 035036 (2022).

[42] M. Ovchynnikov, T. Schwetz, and J.-Y. Zhu, Dipole portal and neutrinophilic scalars at DUNE revisited: The importance of the high-energy neutrino tail, Phys. Rev. D **107**, 055029 (2023).

[43] Y. Zhang, M. Song, R. Ding, and L. Chen, Neutrino dipole portal at electron colliders, Phys. Lett. B **829**, 137116 (2022).

[44] S.-Y. Guo, M. Khlopov, L. Wu, and B. Zhu, Can sterile neutrino explain very high energy photons from GRB221009A?, arXiv:2301.03523.

[45] A. K. Alok, N. R. S. Chundawat, and A. Mandal, Cosmic neutrino flux and spin flavor oscillations in intergalactic medium, Phys. Lett. B **839**, 137791 (2023).

[46] J. M. Butterworth, M. Chala, C. Englert, M. Spannowsky, and A. Titov, Higgs phenomenology as a probe of sterile neutrinos, Phys. Rev. D **100**, 115019 (2019).

[47] CEPC Study Group, CEPC conceptual design report: Volume 1—Accelerator, arXiv:1809.00285.

[48] M. Dong *et al.* (CEPC Study Group), CEPC conceptual design report: Volume 2—Physics & detector, arXiv:1811.10545.

[49] A. Alloul, N. D. Christensen, C. Degrande, C. Duhr, and B. Fuks, FeynRules 2.0—A complete toolbox for tree-level phenomenology, Comput. Phys. Commun. **185**, 2250 (2014).

[50] C. Degrande, C. Duhr, B. Fuks, D. Grellscheid, O. Mattelaer, and T. Reiter, UFO—The universal FeynRules output, Comput. Phys. Commun. **183**, 1201 (2012).

[51] J. Alwall, R. Frederix, S. Frixione, V. Hirschi, F. Maltoni, O. Mattelaer, H.-S. Shao, T. Stelzer, P. Torrielli, and M. Zaro, The automated computation of tree-level and next-to-leading order differential cross sections, and their matching to parton shower simulations, J. High Energy Phys. 07 (2014) 079.

[52] L. F. Li and F. Wilczek, Physical processes involving Majorana neutrinos, Phys. Rev. D **25**, 143 (1982).

[53] M. Masip, P. Masjuan, and D. Meloni, Heavy neutrino decays at MiniBooNE, J. High Energy Phys. 01 (2013) 106.

[54] R. Akers *et al.* (OPAL Collaboration), Measurement of single photon production in $e^+e^-$ collisions near the $Z^0$ resonance, Z. Phys. C **65**, 47 (1995).

[55] DELPHI Collaboration, Photon events with missing energy in $e^+e^-$ collisions at $\sqrt{s} = 130$-GeV to 209-GeV, Eur. Phys. J. C **38**, 395 (2005).

[56] M. Acciarri *et al.* (L3 Collaboration), Search for new physics in energetic single photon production in $e^+e^-$ annihilation at the $Z$ resonance, Phys. Lett. B **412**, 201 (1997).

[57] S. Schael *et al.* (ALEPH, DELPHI, L3, OPAL, SLD Collaborations, LEP Electroweak Working Group, SLD Electroweak Group, SLD Heavy Flavour Group), Precision electroweak measurements on the $Z$ resonance, Phys. Rep. **427**, 257 (2006).

[58] H. Cheng *et al.* (CEPC Physics Study Group), The physics potential of the CEPC. Prepared for the U.S. Snowmass Community Planning Exercise (Snowmass 2021), in 2022 Snowmass Summer Study, (2022), arXiv:2205.08553.

[59] C. Bartels, M. Berggren, and J. List, Characterising WIMPs at a future $e^+e^-$ linear collider, Eur. Phys. J. C **72**, 2213 (2012).

[60] M. Habermehl, M. Berggren, and J. List, WIMP dark matter at the international linear collider, Phys. Rev. D **101**, 075053 (2020).

[61] Z. Liu, Y.-H. Xu, and Y. Zhang, Probing dark matter particles at CEPC, J. High Energy Phys. 06 (2019) 009.

[62] S. N. Gninenko and N. V. Krasnikov, Limits on the magnetic moment of sterile neutrino and two photon neutrino decay, Phys. Lett. B **450**, 165 (1999).

[63] R. Schwienhorst *et al.* (DONUT Collaboration), A new upper limit for the tau-neutrino magnetic moment, Phys. Lett. B **513**, 23 (2001).